

Article

Fabrication of a Nitrogen and Boron-Doped Reduced Graphene Oxide Membrane-Less Amperometric Sensor for Measurement of Dissolved Oxygen in a Microbial Fermentation

Selvaraj Chinnathambi ¹, Sumit Kumar ² and Gert-Jan Willem Euverink ^{1,*}

¹ Products and Processes for Biotechnology, Engineering and Technology Institute Groningen, University of Groningen, Nijenborgh 4, 9747 AG Groningen, The Netherlands; selvarajcg@gmail.com

² Zernike Institute for Advanced Materials, University of Groningen, Nijenborgh 4, 9747 AG Groningen, The Netherlands; Sumit.Kumar@rug.nl

* Correspondence: g.j.w.euverink@rug.nl; Tel.: +31-503-639-203

Received: 18 May 2020; Accepted: 19 June 2020; Published: 22 June 2020



Abstract: Dissolved oxygen (DO) is an important parameter to monitor in processes applicable in, for example, water technology and fermentation. In this study, we report the manufacturing of a membrane-less amperometric sensor that is based on the electrocatalytic reduction of oxygen. The sensor was tested in pH-neutral KNO₃ solutions and in a microbial fermentation to monitor the consumption of dissolved oxygen. The nitrogen and boron-doped reduced graphene oxide (N,B-HRGO) is used as an electrocatalyst for oxygen reduction. One step co-doping of nitrogen and boron on graphene oxide is performed using the hydrothermal method. The sensor responded linearly to the DO concentration. A sensitivity of 0.2 μA/mg·L⁻¹ O₂ is obtained for the DO concentration of 1.5 to 10 mg·L⁻¹ O₂. The membrane-less N,B-HRGO based DO sensor is successfully tested in an *Amycolotopsis methanolica* fermentation by monitoring the dissolved oxygen in real-time. The sensor detected the consumption of oxygen during the growth of *A. methanolica*, which shows the compatibility of N,B-HRGO as electrode material for amperometric measurement of dissolved oxygen in aerobic fermentation. This membrane-less amperometric sensor can be used to fabricate microdevices for microbioreactor applications.

Keywords: dissolved oxygen; nitrogen and boron doping; reduced graphene oxide; amperometric sensor; oxygen reduction; fermentation

1. Introduction

Dissolved oxygen (DO) is an important parameter in various biological and environmental processes like aquatic systems, water quality maintenance and fermentation processes [1]. Electrochemical and optical sensors are commonly used for measuring dissolved oxygen in biological processes. The electrochemical sensors are favorable for DO measurements due to high sensitivity, stability and selectivity. The Clark-type electrochemical sensor is widely used to measure dissolved oxygen [2]. In this sensor, oxygen is reduced at the cathode and silver is oxidized at the anode. The electrodes are separated from the electrolyte by an oxygen-permeable membrane. The current produced by the oxygen reduction reaction (ORR) depends on the concentration of dissolved oxygen present in the electrolyte. However, the size, complex assembly of electrodes with liquid electrolyte and addition of an oxygen-permeable membrane make it challenging to use the electrodes in miniaturized applications, for example, micro-bioreactors. The oxygen-permeable membrane used in the amperometric DO sensor protects the electrode from any interference from redox-active compounds

in the solution and biofouling. In addition to that, it also helps to mitigate the effect of stirring on the sensor response. However, the presence of the membrane increases the response time and complicates the sensor fabrication process. The ultra-microelectrode array (UMEAs) is another method that is used for the construction of an amperometric DO sensor that is insensitive to the stirring of the analytes [3–7]. This is because the detection process is no longer limited by oxygen transport due to a shorter diffusion length. In general, a UMEA is fabricated using a bare platinum electrode, which increases the cost of the sensor in addition to the need for expensive microfabrication techniques. For application in micro-bioreactors, it is an advantage to develop electrode materials that are inexpensive and can be used in a complex biological medium without the requirement of an oxygen-permeable membrane to simplify their construction.

Graphene is a two-dimensional material that has high electronic conductivity and is thermally and chemically stable [8]. Graphene properties can be tuned by functionalizing with different molecules and doping with hetero-atoms [9–16]. Several hetero-atom doped graphenes have been studied as electrocatalysts for the oxygen reduction reaction. The presence of hetero-atoms makes the graphene electron-deficient, which increases the catalytic activity towards the oxygen reduction reaction (ORR) [17–19]. There have been several electrode materials reported for the manufacturing of an amperometric dissolved oxygen sensor [20–36]. Many of the reported materials need electrocatalyst, additional conductive material and a membrane to avoid interference and antifouling activity. However, there are only a few reports available in the literature that investigated graphene-based electrocatalysts as electrode material for amperometric detection of dissolved oxygen. An amine and carboxylic acid functionalized graphene was reported as the electrode material in a DO sensor [37]. A Teflon based membrane was used and the reported sensitivity was $1.026 \text{ nA/mg}\cdot\text{L}^{-1} \text{ O}_2$. Saravia et al. described a sensor based on Co-porphyrin (Co-TRP) modified graphene oxide composite and achieved a limit of detection (LOD) of $0.19 \text{ mg}\cdot\text{L}^{-1} \text{ O}_2$ [38]. However, these sensors were tested in a simple electrolyte solution and the applicability of these electrode materials in a complex medium is not known. In this study, we investigated nitrogen and boron-doped reduced graphene oxide as electrode material for application in an amperometric dissolved oxygen sensor. The main advantage of this metal-free N,B-doped reduced graphene oxide as an electrode material is that these materials are cheap and have high chemical stability to withstand harsh environments. Previously, the electrocatalytic activity of nitrogen and boron-doped graphene was studied in alkaline and acidic medium [17,39] but the activity in pH-neutral electrolytes is unknown. The feasibility of the sensor to detect dissolved oxygen during a fermentation process with *Amycalotopsis methanolica* was investigated here. The sensor was able to detect the consumption of dissolved oxygen in a complex fermentation medium during bacterial growth. Importantly, the sensor works without the need for an oxygen-permeable membrane, which demonstrates the advantage in further miniaturizing the sensor for microbioreactor applications.

2. Materials and Methods

2.1. Material Preparation

N,B-HRGO was synthesized through a one-step co-doping process using a hydrothermal method, as reported earlier [40,41]. In a typical procedure, 50 mg of graphite oxide was dispersed in 50 mL ultrapure water [42–44]. The dispersion was sonicated for six hours and un-exfoliated graphite oxide flakes were removed by centrifugation. The resultant GO dispersion was used for functionalization. For nitrogen and boron doping, 5 mL (25%) NH_3 and 7.2 g boric acid (H_3BO_3) were dissolved in 50 mL GO dispersion and autoclaved for 12 h at $120 \text{ }^\circ\text{C}$ (0.12 MPa). In the initial brown GO dispersion, black solids were formed during the hydrotreatment. The solids (N,B-HRGO) were collected by vacuum filtration (Figure 1a,b).

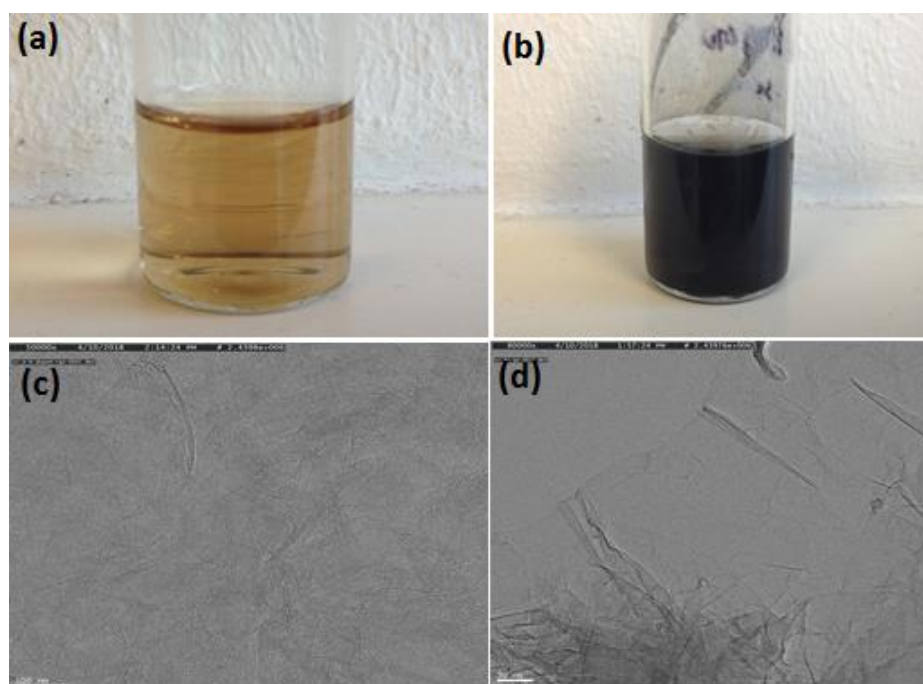


Figure 1. Photos of graphene oxide before (a) and after (b) nitrogen and boron doping. Transmission electron microscopy (TEM) image of GO (c) and N,B-HRGO (d).

For the growth of *A. methanolica*, 50 mL of the culture medium was prepared by mixing 0.5 mL of glucose (1 M), 0.5 mL of ammonium sulfate ($100 \text{ g}\cdot\text{L}^{-1}$), 0.5 mL of magnesium chloride ($20 \text{ g}\cdot\text{L}^{-1}$), 5 mL of phosphate buffer (K_2HPO_4 [$47 \text{ g}\cdot\text{L}^{-1}$] and NaH_2PO_4 [$15 \text{ g}\cdot\text{L}^{-1}$]) and 0.05 mL of Vishniac trace element solution in 43.5 mL of demineralized water. All the solutions were separately sterilized before use. The inoculated growth medium containing an electrochemical cell was placed in a thermostat at $30 \text{ }^\circ\text{C}$. The lid of the electrochemical cell containing the culture was modified to accommodate a commercial DO sensor and the N,B-HRGO electrode. During the growth, 1 mL samples were taken from the culture using a sterilized syringe to monitor the growth of *A. methanolica* by offline optical turbidity measurements at 600 nm.

2.2. Instruments and Methodology

For the amperometric sensor, a 2 mm gold disc, a platinum wire and an Ag/AgCl with saturated KCl electrolyte were used as working, counter and reference electrode, respectively. The electrochemical measurements were performed with a potentiostat (CH760, CH instruments, Austin, TX, USA). A three-compartment electrochemical cell was used for electrochemical measurements. For the electrode fabrication, 2 μL of 1 mg/mL N,B-HRGO dispersion was drop-cast on a pre-cleaned gold electrode. Then, the electrode was dried in an oven at $101 \text{ }^\circ\text{C}$ for 24 h. For amperometric sensing, a -0.4 V constant potential was applied to the electrode and the current was measured against time. For dissolved oxygen sensing, the amperometric response was obtained in 0.1 M KNO_3 solution purged with oxygen. For continuous DO sensing, the electrolyte was saturated with pure O_2 and N_2 gas bubbling. The flow of O_2 and/or N_2 gas was stopped (after a stable current response was reached) at various intervals to obtain stable and varying DO concentrations. The actual DO concentration of the 0.1 M KNO_3 solution was measured with a commercial DO sensor (Greisinger GOX20 Oxymeter).

X-ray Photoelectron Spectroscopy (XPS) was performed using a Surface Science SSX-100 ESCA instrument with a monochromatic Al K_α X-ray source ($h\nu = 1486.6 \text{ eV}$). The constant chamber pressure was below 2×10^{-9} mbar during data acquisition. The take-off angle of electrons with respect to the surface normal was $37 \text{ }^\circ\text{C}$. The diameter of the analyzed area was 1 mm yielding a total experimental energy resolution of 1.1 eV. Binding energies are reported $\pm 0.1 \text{ eV}$ and referenced to the Au $4f_{7/2}$

photoemission peak originating from the substrate, centered at a binding energy of 84 eV. All the samples were prepared in water by mild sonication, a small drop of the suspension was left to dry in the air on a 100 nm thick gold-on-mica substrate. The spectral analysis included a Shirley background subtraction and peak deconvolution employing mixed Gaussian–Lorentzian functions in a least-squares curve-fitting program (WinSpec) developed at the LISE, University of Namur, Namur, Belgium.

Transmission electron microscopy (TEM) was carried out at 120 keV (CM12, Philips, Eindhoven, The Netherlands). The samples were prepared on a carbon-coated 400 mesh copper grid and the images were recorded with a slow-scan CCD camera.

3. Results and Discussion

3.1. Material and Electrochemical Characterization

The TEM images of the N,B-HRGO and GO are shown in Figure 1c,d. The TEM image of GO showed a thin film of single-layer graphene oxide sheets. The TEM image of N,B-HRGO also showed a similar film but with more wrinkles after the reduction and doping process (Figure 1c,d). The formation of nitrogen and boron doping was confirmed by X-ray photoelectron spectroscopy (Figure 2). The C1s core-level region of GO and N,B-HRGO is shown in Figure 2a,b. The three main peaks for GO at 284.4 eV [45], 286.3 eV [46] and 288.4 eV [47] correspond to aliphatic C-C, C=O/C-O and COO. The additional peak at 292.5 eV is indicative of π - π^* . In the case of N,B-HRGO, the peak intensity at 286.3 eV decreased due to the reduction of C=O/C-O. Two additional peaks at 283.9 eV [48] and 285.4 eV [45] appeared, corresponding to C-B and C-N. N1s and B1s deconvoluted spectra in Figure 2c,d show the different binding states of N and B in N,B-HRGO. The peaks at 398.8 eV [45], 400.0 eV [45,49] and 401.7 eV [49] in N1s spectra correspond to pyridinic, pyrrolic and graphitic nitrogen, respectively. The peaks at 191.1 eV [46], 191.7 eV [50] and 192.3 eV [41] attributed to the presence of B-C₃, B-C-O and B-O, respectively.

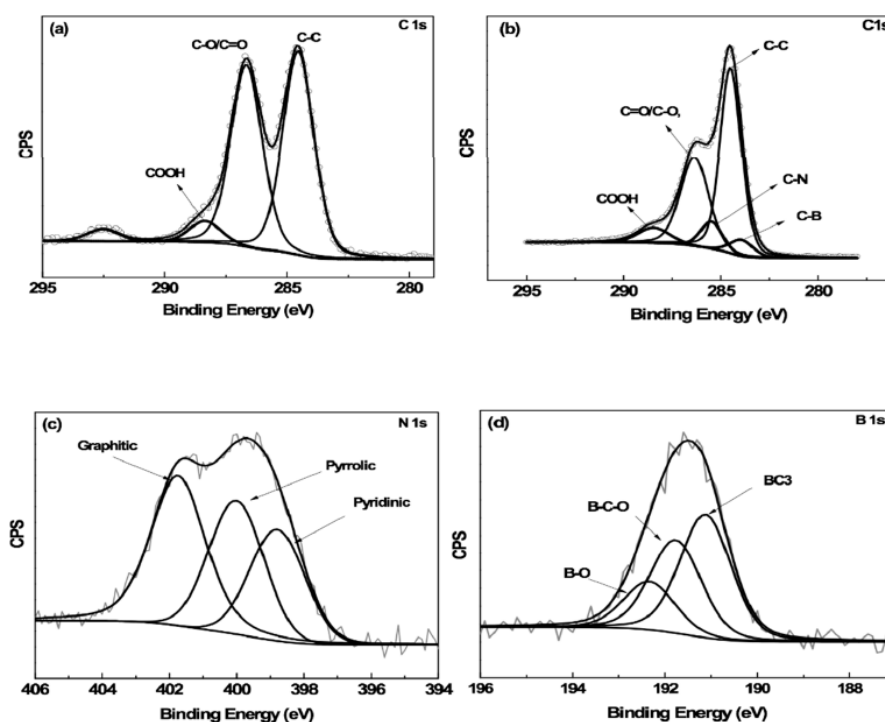


Figure 2. X-ray Photoelectron Spectroscopy (XPS) spectra of GO and N,B-HRGO. Deconvoluted C1s spectra of GO (a) and C1s (b), N1s (c) and B1s (d) spectra of N,B-HRGO.

3.2. Electrocatalytic Activity

The electrocatalytic activity of N,B-HRGO for the oxygen reduction reaction in 0.1 M KNO₃ at neutral pH was evaluated by cyclic voltammetry (CV) (Figure 3a). The voltage over the electrode was cycled between 0 and −1.0 V at a scan rate of 50 mV/s. The CV of N,B-HRGO showed a sharp oxygen reduction peak at −0.3 V with an onset potential of less than −0.1 V. This peak completely disappeared when the electrolyte was purged with nitrogen gas. This indicates that N,B-HRGO has good electrocatalytic activity towards the oxygen reduction reaction and might be used to amperometrically detect dissolved oxygen with high sensitivity and selectivity. The schematic of the oxygen reduction reaction at the N,B-HRGO electrode is shown in Figure 3b.

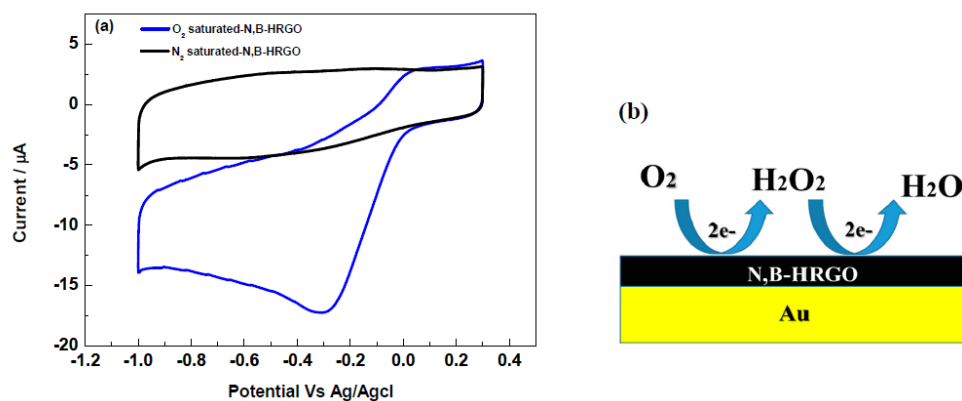


Figure 3. Cyclic voltammetry of N,B-HRGO in nitrogen saturated (black) and oxygen saturated (blue) 0.1M KNO₃ solution (a). The schematic of the oxygen reduction reaction at the N,B-HRGO electrode (b); Au–Gold disc electrode.

3.3. Amperometric Sensing of Dissolved Oxygen

The amperometric sensor measurement was carried out at an applied potential of −0.4 V and the oxygen reduction (cathodic) current was monitored as the sensor response. To detect the dissolved oxygen in real-time, the amperometric response of the N,B-HRGO electrode was continuously recorded while the DO concentration was changed by nitrogen gas bubbling. In Figure 4a, the continuous amperometric response of the N,B-HRGO electrode in 0.1 M KNO₃, is shown. As a reference, the DO concentration was measured with a commercial DO sensor. The de-aeration of the solution with N₂ gas was started after the electrode reached a stable current. N₂ purging decreased the concentration of DO and changed the response of the electrode, as the current depends on the DO concentration. The initial DO concentration measured with a commercial DO meter was 8.8 mg·L^{−1} O₂ and at the end of the N₂ bubbling, it was 1.5 mg·L^{−1} O₂. The N₂ gas bubbling was stopped at a DO concentration of 1.5 mg·L^{−1} because in our setup, it was difficult to remove oxygen from the solution below 1.5 mg·L^{−1} O₂. As expected, during the N₂ bubbling, the current decreased and became constant at 1.5 mg·L^{−1} when N₂ purging was stopped (Figure 4a). The sensitivity and the response time of the N,B-HRGO electrode at various DO concentration is shown in Figure 4b. The amperometric response of the N,B-HRGO electrode at different DO concentration was examined at the same applied potential of −0.4 V. To obtain a specific DO level, alternating O₂ and N₂ bubbling was performed. The bubbling of N₂ or O₂ gas was stopped at the desired DO level and maintained until the electrode reached a stable current. It is important to note that the electrode responded immediately to the change of DO concentration, which shows that the N,B-HRGO electrode has good sensitivity and fast response time. The current changed linearly with DO concentration and a sensitivity of 0.2 µA/mg·L^{−1} O₂ was obtained in the range from 1.5 to 10.0 mg·L^{−1} O₂ (Figure 4c). The limit of detection (LOD, calculated from the signal to noise ratio and the slope of the DO measurement curve.) was estimated to be 0.1 mg L^{−1} O₂. The electrode showed a similar response when the DO concentration was switched back from 10.0 to 1.5 mg L^{−1} O₂.

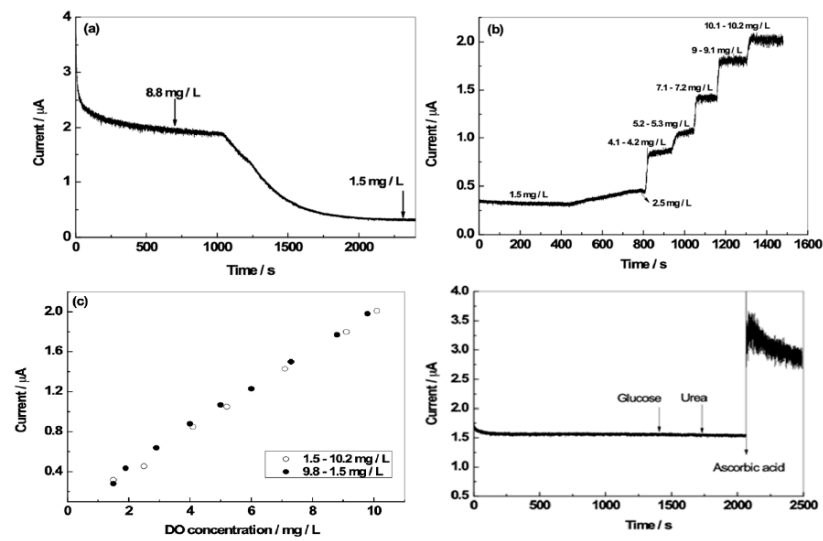


Figure 4. Dissolved oxygen (DO) sensing of N,B-HRGO electrode. (a): Amperometric response of N,B-HRGO during nitrogen purging, initial DO concentration of $8.8 \text{ mg}\cdot\text{L}^{-1} \text{ O}_2$ and final DO concentration of $1.5 \text{ mg}\cdot\text{L}^{-1}$. (b): Amperometric response at varying DO concentration. (c): calibration curve for N,B-HRGO electrode. (d): sensor response after the subsequent addition of glucose, urea and ascorbic acid (each 1 mM).

The sensor measurement for each electrode was repeated four times with alternate increasing and decreasing DO concentration (two cycles of a one-cycle experiment are shown in Figure 4c) and reproducible current values were obtained. The performance of the sensor is comparable with other reported work, which is shown in Table 1.

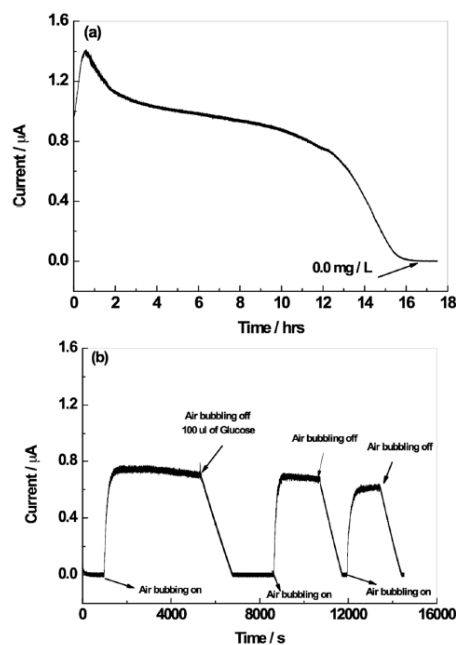


Figure 5. Real-time DO measurement with the N,B-HRGO electrode during an *Amycolatopsis methanolica* fermentation (a). N,B-HRGO electrode response during repeated exposure of the growth medium to dissolved oxygen (b).

Table 1. Comparison with other existing amperometric dissolved oxygen sensor.

Sensor Material	Potential (V)	Limit of Detection	Linear Response Range	Sensitivity	Ref.
N,B-HRGO ¹	-0.4	0.1 mg/L	1.5–10.0 mg/L	0.2 $\mu\text{A L mg}^{-1}$	This work
CoTRP/GO ²	-0.05	0.19 mg/L	0–21.24 mg/L	0.104 mA cm^{-2}	[38]
Hemin/polypyrrole/Ag ³	-0.7	-	2–7 mg/L	8.5 $\mu\text{A L mg}^{-1}$	[27]
Nickel/Salen/Platinum ⁴	-0.25	0.17 mg/L ⁻¹	3.95–9.2 mg/L	0.9 $\mu\text{A L mg}^{-1}$	[23]
Graphene/Ag ⁵	-0.3	0.031 μM	1–120 μM	0.205 $\mu\text{A } \mu\text{mol}^{-1}$	[31]
Au-BDD ⁶	-0.5	4 mg/L	10–50 mg/L	1.4 $\mu\text{A L mg}^{-1}$	[22]
Au nanoparticles (IPE) ⁷	-	0.11 mg/L	0–8 mg/L	0.03 $\mu\text{A L mg}^{-1}$	[24]
[Cu ₄ (apyhist) ₄] ⁴⁺ /FF-MNT-coated/GCE ⁸	-0.4	0.1 mg/L	0.2–3.0 mg/L	25 $\mu\text{A cm}^{-2} \text{ L mg}^{-1}$	[28]
HOOC-2 AQ/AMWCNTs ⁹	-0.518	0.02 mg/L	0.2–6.8 mg/L	5 $\mu\text{A L mg}^{-1}$	[36]
GNP/MWCNTs-FeTMAPP ¹⁰	-0.25	0.01 mg/L	0.01–5.8 mg/L	59.4 $\mu\text{A mM}^{-1}$	[33]
SiO ₂ /SnO ₂ /MnPc ¹¹	-0.3	0.02 mg/L	0–253 $\mu\text{M/L}$	0.147 $\mu\text{A L } \mu\text{mol}^{-1}$	[35]
β CDSH/FeTMPyP/CDAuNP ¹²	-0.15	0.02 mg/L	0.2–6.5 mg/L	5.5 $\mu\text{A L mg}^{-1}$	[29]
poly(Nile blue)/GCE ⁸	-	0.01 mg/L	0.02–0.4 mg/L	-	[32]
cobalt tetrasulfonated phthalocyanine/poly-L-lysine	-0.16	0.09 mg/L	0.2–8 mg/L	11 $\mu\text{A cm}^{-2} \text{ L mg}^{-1}$	[34]
FeTsPc/FeT4MPyP ¹³	-0.15	0.06 mg/L	0.2–6.4 mg/L	4.12 $\mu\text{A L mg}^{-1}$	[30]

Nitrogen, boron doped hydrothermally reduced graphene oxide (N,B-HRGO)¹; [tetrakis-bisdimethylbipyridine-chlororuthenium(II)]-5,10,15,20-tetrapyridylporphyrinatecobalt complex (CoTRP)/Graphene oxide (GO)²; Silver (Ag)^{3,5}; N,N'-ethylenebis(salicylideneiminato) (Salen)⁴; Boron doped Diamond (BDD)⁶; Ink-jet printed electrodes (IPE)⁷; Cyclic-tetrameric copper(II) species containing the ligand (4-imidazolyl)ethylene-2-amino-1-ethylpyridine (apyhist) self-assembled with L-diphenylalanine micro/nanostructures ([Cu₄(apyhist)₄]⁴⁺/FF-MNT)⁸; glassy carbon electrode (GCE)⁸; Nanowires of (anthraquinone-2-carboxylic acid/amino functionalized) multiwalled carbon nanotubes (HOOC-2-AQ/AMWCNTs)⁹; Multiwalled carbon nanotubes (MWCNTs)⁹; Gold nanoparticles (GNP)¹⁰; Iron picket-fence porphyrin (FeTMAPP)¹⁰; Manganese(II) phthalocyanine (MnPc)¹¹; Mono-(6-deoxy-6-mercapto)- β -cyclodextrin (β CDSH)¹²; Iron(III) tetra-(N-methyl-4-pyridyl)-porphyrin (FeTMPyP)¹²; Cyclodextrin-functionalized gold nanoparticles (CDAuNP)¹²; Iron(III) tetra-(N-methyl-pyridyl)-porphyrin (FeT4MPyP)¹³; Iron(II) tetrasulfonated phthalocyanine (FeTsPc)¹³.

The amperometric response of the N,B-HRGO electrode in the presence of the physiologically important molecules that have the potential to interfere with the amperometric signal was also tested. Figure 4d shows the amperometric response of the electrode in the presence of glucose, urea and ascorbic acid. There was no interference observed for glucose (10 mM) and urea(10 mM). However, in the presence of ascorbic acid even at 1 mM, a substantial interference occurred (Figure 4d).

3.4. Real-Time Monitoring of Dissolved Oxygen during the Growth of *Amycalotopsis methanolica*

To demonstrate the feasibility of the sensor to use in real applications, the amperometric response of the N,B-HRGO electrode to detect dissolved oxygen during the growth of *A. methanolica* fermentation was tested. The presence of oxygen in the growth medium is essential for the growth of *A. methanolica*. The amperometric response of the N,B-HRGO electrode during the growth of *A. methanolica* is shown in Figure 5a. The sensor response is stable during the lag phase in which growth is not yet started and decreased exponentially during the subsequent exponential growth phase. When the bacteria completely consumed the oxygen, the growth ceased and the sensor response stabilized at 0 mg·L⁻¹ O₂. The stability and reproducibility of the sensor in the complex fermentation medium were also explored. After *A. methanolica* consumed the oxygen, air was bubbled through the growth medium until the DO concentration reached 6.6 mg·L⁻¹ O₂ (Figure 5b). The bacteria immediately consumed the newly supplied O₂ and reduced the DO concentration in the growth medium. The electrode quickly responded to this rapid change in DO concentration. This procedure was repeated two more times and the electrode responded reproducibly to this alternating O₂ supply and O₂ consumption. The limitation of the carbon-source was prevented by the addition of 100 μL of 1 M glucose after the first cycle, immediately after the air bubbling was stopped (arrow in Figure 5b shows the time of addition). It is worth mentioning that the electrode detected oxygen in the fermentation medium without the need for an oxygen-permeable membrane to prevent that unwanted side-reactions take place at the electrocatalytic surface. Moreover, the demonstrated sensitivity, stability and fast response time of the N,B-HRGO electrode in a 0.1 M KNO₃ solution and complex growth medium showed that the

electrode could be used as an amperometric sensor for real-time monitoring of dissolved oxygen in fermentations.

4. Conclusions

Nitrogen and boron-doped reduced graphene oxide was studied as an electrode material for amperometric detection of dissolved oxygen. Cyclic voltammetry was used to evaluate the electrocatalytic activity of N,B-HRGO, in a neutral electrolyte. The amperometric sensing method was used to detect dissolved oxygen in 0.1 M KNO₃. The sensitivity of 0.2 μA/mg·L⁻¹ O₂ was calculated for a DO concentration between 1.5 and 10.0 mg·L⁻¹ O₂. The applicability of the sensor in microbial fermentation was also tested using the aerobic bacterium *A. methanolica*. The response of the sensor correlated nicely with the oxygen consumption of the bacteria during the growth. The electrode without an oxygen-permeable membrane was tested in a complex fermentation medium. We showed that the (redox-active) components in the fermentation medium did not interfere with the measurements of DO using the N,B-HRGO electrode.

Author Contributions: The work was conceptualized by S.C. and G.-J.W.E. The authors S.C. and G.-J.W.E. were involved in all aspects of the work. S.K. contributed to XPS methodology, data curation, analysis and validation. All other experimental work was carried out by S.C. The writing of the original draft was prepared by S.C. The work is supervised and validated by G.-J.W.E. and also involved in writing, reviewing and editing the manuscript. All authors have read and agreed to the published version of the manuscript.

Funding: This research received no external funding.

Acknowledgments: The authors thank A.M. Stuart for the TEM images of the different electrode materials.

Conflicts of Interest: The authors declare no conflict of interest.

References

1. Mills, A. Oxygen indicators and intelligent inks for packaging food. *Chem. Soc. Rev.* **2005**, *34*, 1003–1011. [[CrossRef](#)] [[PubMed](#)]
2. Clark, J.R.L.C.; Misrahy, G.; Fox, R.P. Chronically implanted polarographic electrodes. *J. Appl. Physiol.* **1958**, *13*, 85–91. [[CrossRef](#)]
3. Krommenhoek, E.; Gardeniers, J.G.; Bomer, J.G.; Li, X.; Ottens, M.; Van Dedem, G.; Van Leeuwen, M.; Van Gulik, W.; Van Der Wielen, L.; Heijnen, J. Integrated electrochemical sensor array for on-line monitoring of yeast fermentations. *Anal. Chem.* **2007**, *79*, 5567–5573. [[CrossRef](#)]
4. Lee, J.-H.; Lim, T.-S.; Seo, Y.; Bishop, P.L.; Papautsky, I. Needle-type dissolved oxygen microelectrode array sensors for in situ measurements. *Sens. Actuators B Chem.* **2007**, *128*, 179–185. [[CrossRef](#)]
5. Ordeig, O.; del Campo, J.; Munoz, F.X.; Banks, C.E.; Compton, R.G. Electroanalysis utilizing amperometric microdisk electrode arrays. *Electroanal. Int. J. Devoted Fundam. Pract. Asp. Electroanal.* **2007**, *19*, 1973–1986. [[CrossRef](#)]
6. Orozco, J.; Fernández-Sánchez, C.; Jiménez-Jorquera, C. Ultramicroelectrode array based sensors: A promising analytical tool for environmental monitoring. *Sensors* **2010**, *10*, 475–490. [[CrossRef](#)]
7. van Rossem, F.; Bomer, J.G.; de Boer, H.L.; Abbas, Y.; de Weerd, E.; van den Berg, A.; Le Gac, S. Sensing oxygen at the millisecond time-scale using an ultra-microelectrode array (UMEA). *Sens. Actuators B Chem.* **2017**, *238*, 1008–1016. [[CrossRef](#)]
8. Novoselov, K.S.; Geim, A. The rise of graphene. *Nat. Mater* **2007**, *6*, 183–191.
9. Liang, J.; Jiao, Y.; Jaroniec, M.; Qiao, S.Z. Sulfur and nitrogen dual-doped mesoporous graphene electrocatalyst for oxygen reduction with synergistically enhanced performance. *Angew. Chem. Int. Ed.* **2012**, *51*, 11496–11500. [[CrossRef](#)]
10. Liu, Z.W.; Peng, F.; Wang, H.J.; Yu, H.; Zheng, W.X.; Yang, J. Phosphorus-doped graphite layers with high electrocatalytic activity for the O₂ reduction in an alkaline medium. *Angew. Chem. Int. Ed.* **2011**, *50*, 3257–3261. [[CrossRef](#)]
11. Qu, L.; Liu, Y.; Baek, J.-B.; Dai, L. Nitrogen-doped graphene as efficient metal-free electrocatalyst for oxygen reduction in fuel cells. *ACS Nano* **2010**, *4*, 1321–1326. [[CrossRef](#)] [[PubMed](#)]

12. Sheng, Z.-H.; Gao, H.-L.; Bao, W.-J.; Wang, F.-B.; Xia, X.-H. Synthesis of boron doped graphene for oxygen reduction reaction in fuel cells. *J. Mater. Chem.* **2012**, *22*, 390–395. [[CrossRef](#)]
13. Wang, S.; Zhang, L.; Xia, Z.; Roy, A.; Chang, D.W.; Baek, J.B.; Dai, L. BCN graphene as efficient metal-free electrocatalyst for the oxygen reduction reaction. *Angew. Chem. Int. Ed.* **2012**, *51*, 4209–4212. [[CrossRef](#)] [[PubMed](#)]
14. Yang, Z.; Yao, Z.; Li, G.; Fang, G.; Nie, H.; Liu, Z.; Zhou, X.; Chen, X.A.; Huang, S. Sulfur-doped graphene as an efficient metal-free cathode catalyst for oxygen reduction. *ACS Nano* **2012**, *6*, 205–211. [[CrossRef](#)]
15. Yao, Z.; Nie, H.; Yang, Z.; Zhou, X.; Liu, Z.; Huang, S. Catalyst-free synthesis of iodine-doped graphene via a facile thermal annealing process and its use for electrocatalytic oxygen reduction in an alkaline medium. *Chem. Commun.* **2012**, *48*, 1027–1029. [[CrossRef](#)]
16. Zheng, Y.; Jiao, Y.; Ge, L.; Jaroniec, M.; Qiao, S.Z. Two-step boron and nitrogen doping in graphene for enhanced synergistic catalysis. *Angew. Chem. Int. Ed.* **2013**, *52*, 3110–3116. [[CrossRef](#)]
17. Gong, K.; Du, F.; Xia, Z.; Durstock, M.; Dai, L. Nitrogen-doped carbon nanotube arrays with high electrocatalytic activity for oxygen reduction. *Science* **2009**, *323*, 760–764. [[CrossRef](#)]
18. Ikeda, T.; Boero, M.; Huang, S.-F.; Terakura, K.; Oshima, M.; Ozaki, J.-I. Carbon alloy catalysts: Active sites for oxygen reduction reaction. *J. Phys. Chem. C* **2008**, *112*, 14706–14709. [[CrossRef](#)]
19. Radovic, L.R.; Karra, M.; Skokova, K.; Thrower, P.A. The role of substitutional boron in carbon oxidation. *Carbon* **1998**, *36*, 1841–1854. [[CrossRef](#)]
20. Devi, K.S.; Jain, A.; Huang, S.-T.; Kumar, A.S. Metal and heteroatoms-free carbon soot obtained from atmospheric combustion of naphthalene for sensitive dissolved oxygen reduction reaction and sensing in neutral media. *Electrochim. Acta* **2019**, *296*, 407–417. [[CrossRef](#)]
21. Hutton, L.; Newton, M.E.; Unwin, P.R.; Macpherson, J.V. Amperometric oxygen sensor based on a platinum nanoparticle-modified polycrystalline boron doped diamond disk electrode. *Anal. Chem.* **2009**, *81*, 1023–1032. [[CrossRef](#)] [[PubMed](#)]
22. Ivandini, T.A.; Saepudin, E.; Wardah, H.; Dewangga, N.; Einaga, Y. Development of a biochemical oxygen demand sensor using gold-modified boron doped diamond electrodes. *Anal. Chem.* **2012**, *84*, 9825–9832. [[CrossRef](#)] [[PubMed](#)]
23. Martin, C.S.; Damos, T.R.; Teixeira, M.F. Development of an electrochemical sensor for determination of dissolved oxygen by nickel–salen polymeric film modified electrode. *Sens. Actuators B Chem.* **2012**, *175*, 111–117. [[CrossRef](#)]
24. Moya, A.; Sowade, E.; del Campo, F.J.; Mitra, K.Y.; Ramon, E.; Villa, R.; Baumann, R.R.; Gabriel, G. All-inkjet-printed dissolved oxygen sensors on flexible plastic substrates. *Org. Electron.* **2016**, *39*, 168–176. [[CrossRef](#)]
25. Saravia, L.P.H.; Anandhakumar, S.; Parússulo, A.L.A.; Matias, T.A.; da Silva, C.C.; Kowaltowski, A.J.; Araki, K.; Bertotti, M. Development of a tetraphenylporphyrin cobalt (II) modified glassy carbon electrode to monitor oxygen consumption in biological samples. *J. Electroanal. Chem.* **2016**, *775*, 72–76. [[CrossRef](#)]
26. Tiwari, I.; Gupta, M.; Prakash, R.; Banks, C.E. An anthraquinone moiety/cysteamine functionalized-gold nanoparticle/chitosan based nanostructured composite for the electroanalytical detection of dissolved oxygen within aqueous media. *Anal. Methods* **2014**, *6*, 8793–8801. [[CrossRef](#)]
27. Hsu, L.; Selvaganapathy, P.R.; Brash, J.; Fang, Q.; Xu, C.-Q.; Deen, M.J.; Chen, H. Development of a Low-Cost Hemin-Based Dissolved Oxygen Sensor With Anti-Biofouling Coating for Water Monitoring. *IEEE Sens. J.* **2014**, *14*, 3400–3407. [[CrossRef](#)]
28. Sousa, C.P.; Coutinho-Neto, M.D.; Liberato, M.S.; Kubota, L.T.; Alves, W.A. Self-Assembly of Peptide Nanostructures onto an Electrode Surface for Nonenzymatic Oxygen Sensing. *J. Phys. Chem. C* **2014**, *119*, 1038–1046. [[CrossRef](#)]
29. Damos, F.S.; Luz, R.C.; Tanaka, A.A.; Kubota, L.T. Dissolved oxygen amperometric sensor based on layer-by-layer assembly using host–guest supramolecular interactions. *Anal. Chim. Acta* **2010**, *664*, 144–150. [[CrossRef](#)]
30. Duarte, J.C.; Luz, R.C.; Damos, F.S.; Tanaka, A.A.; Kubota, L.T. A highly sensitive amperometric sensor for oxygen based on iron (II) tetrasulfonated phthalocyanine and iron (III) tetra-(N-methyl-pyridyl)-porphyrin multilayers. *Anal. Chim. Acta* **2008**, *612*, 29–36. [[CrossRef](#)]
31. Fu, L.; Zheng, Y.; Fu, Z.; Wang, A.; Cai, W. Dissolved oxygen detection by galvanic displacement-induced graphene/silver nanocomposite. *Bull. Mater. Sci.* **2015**, *38*, 611–616. [[CrossRef](#)]

32. Ju, H.; Shen, C. Electrocatalytic reduction and determination of dissolved oxygen at a poly (nile blue) modified electrode. *Electroanal. Int. J. Devoted Fundam. Pract. Asp. Electroanal.* **2001**, *13*, 789–793. [[CrossRef](#)]
33. Liu, Y.; Yan, Y.-L.; Lei, J.; Wu, F.; Ju, H. Functional multiwalled carbon nanotube nanocomposite with iron picket-fence porphyrin and its electrocatalytic behavior. *Electrochem. Commun.* **2007**, *9*, 2564–2570. [[CrossRef](#)]
34. Luz, R.d.C.S.; Damos, F.S.; Tanaka, A.A.; Kubota, L.T. Dissolved oxygen sensor based on cobalt tetrasulphonated phthalocyanine immobilized in poly-l-lysine film onto glassy carbon electrode. *Sens. Actuators B Chem.* **2006**, *114*, 1019–1027. [[CrossRef](#)]
35. Santos, L.S.; Landers, R.; Gushikem, Y. Application of manganese (II) phthalocyanine synthesized in situ in the SiO₂/SnO₂ mixed oxide matrix for determination of dissolved oxygen by electrochemical techniques. *Talanta* **2011**, *85*, 1213–1216. [[CrossRef](#)] [[PubMed](#)]
36. Tiwari, I.; Singh, M.; Gupta, M.; Aggarwal, S. Electroanalytical properties and application of anthraquinone derivative-functionalized multiwalled carbon nanotubes nanowires modified glassy carbon electrode in the determination of dissolved oxygen. *Mater. Res. Bull.* **2012**, *47*, 1697–1703. [[CrossRef](#)]
37. Wang, J.; Bian, C.; Tong, J.; Sun, J.; Li, Y.; Hong, W.; Xia, S. Modification of Graphene on Ultramicroelectrode Array and Its Application in Detection of Dissolved Oxygen. *Sensors* **2015**, *15*, 382–393. [[CrossRef](#)] [[PubMed](#)]
38. Saravia, L.P.; Sukeri, A.; Gonçalves, J.M.; Aguirre-Araque, J.S.; Brandão, B.B.; Matias, T.A.; Nakamura, M.; Araki, K.; Toma, H.E.; Bertotti, M. CoTRP/Graphene oxide composite as efficient electrode material for dissolved oxygen sensors. *Electrochim. Acta* **2016**, *222*, 1682–1690. [[CrossRef](#)]
39. Wang, S.; Iyyamperumal, E.; Roy, A.; Xue, Y.; Yu, D.; Dai, L. Vertically aligned BCN nanotubes as efficient metal-free electrocatalysts for the oxygen reduction reaction: A synergetic effect by co-doping with boron and nitrogen. *Angew. Chem. Int. Ed.* **2011**, *50*, 11756–11760. [[CrossRef](#)]
40. Jiang, Z.; Zhao, X.; Tian, X.; Luo, L.; Fang, J.; Gao, H.; Jiang, Z.-J. Hydrothermal synthesis of boron and nitrogen codoped hollow graphene microspheres with enhanced electrocatalytic activity for oxygen reduction reaction. *ACS Appl. Mater. Interfaces* **2015**, *7*, 19398–19407. [[CrossRef](#)]
41. Zhou, Y.; Bao, Q.; Tang, L.A.L.; Zhong, Y.; Loh, K.P. Hydrothermal dehydration for the “green” reduction of exfoliated graphene oxide to graphene and demonstration of tunable optical limiting properties. *Chem. Mater.* **2009**, *21*, 2950–2956. [[CrossRef](#)]
42. Chinnathambi, S.; Euverink, G.J.W. Polyaniline functionalized electrochemically reduced graphene oxide chemiresistive sensor to monitor the pH in real time during microbial fermentations. *Sens. Actuators B Chem.* **2018**, *264*, 38–44. [[CrossRef](#)]
43. Hummers, W.S., Jr.; Offeman, R.E. Preparation of graphitic oxide. *J. Am. Chem. Soc.* **1958**, *80*, 1339. [[CrossRef](#)]
44. Selvaraj, C.; Kumar, S.; Munichandraiah, N.; Scanlon, L.G. Reduced Graphene Oxide-Polypyrrole Composite as a Catalyst for Oxygen Electrode of High Rate Rechargeable Li-O₂ Cells. *J. Electrochem. Soc.* **2014**, *161*, A554–A560. [[CrossRef](#)]
45. Li, J.; Li, X.; Zhao, P.; Lei, D.Y.; Li, W.; Bai, J.; Ren, Z.; Xu, X. Searching for magnetism in pyrrolic N-doped graphene synthesized via hydrothermal reaction. *Carbon* **2015**, *84*, 460–468. [[CrossRef](#)]
46. Wang, H.; Zhou, Y.; Wu, D.; Liao, L.; Zhao, S.; Peng, H.; Liu, Z. Synthesis of boron-doped graphene monolayers using the sole solid feedstock by chemical vapor deposition. *Small* **2013**, *9*, 1316–1320. [[CrossRef](#)]
47. Spyrou, K.; Calvaresi, M.; Diamanti, E.K.; Tsoufis, T.; Gournis, D.; Rudolf, P.; Zerbetto, F. Graphite oxide and aromatic amines: Size matters. *Adv. Funct. Mater.* **2015**, *25*, 263–269. [[CrossRef](#)]
48. Li, S.; Wang, Z.; Jiang, H.; Zhang, L.; Ren, J.; Zheng, M.; Dong, L.; Sun, L. Plasma-induced highly efficient synthesis of boron doped reduced graphene oxide for supercapacitors. *Chem. Commun.* **2016**, *52*, 10988–10991. [[CrossRef](#)]
49. Yadav, R.; Dixit, C. Synthesis, characterization and prospective applications of nitrogen-doped graphene: A short review. *J. Sci. Adv. Mater. Devices* **2017**, *2*, 141–149. [[CrossRef](#)]
50. Zehtab Yazdi, A.; Fei, H.; Ye, R.; Wang, G.; Tour, J.; Sundararaj, U. Boron/nitrogen co-doped helically unzipped multiwalled carbon nanotubes as efficient electrocatalyst for oxygen reduction. *ACS Appl. Mater. Interfaces* **2015**, *7*, 7786–7794. [[CrossRef](#)]

